

Article

Effects of HCM cTnI Mutation R145G on Troponin Structure and Modulation by PKA Phosphorylation Elucidated by Molecular Dynamics Simulations

Steffen Lindert,^{1,4,*} Yuanhua Cheng,⁵ Peter Kekenyes-Huskey,^{1,6} Michael Regnier,⁵ and J. Andrew McCammon^{1,2,3,4}¹Department of Pharmacology, ²Howard Hughes Medical Institute, and ³Department of Chemistry and Biochemistry, National Biomedical Computation Resource, University of California San Diego, La Jolla, California; ⁴NSF Center for Theoretical Biological Physics, La Jolla, California; ⁵Department of Bioengineering, University of Washington, Seattle, Washington; and ⁶Department of Chemistry, University of Kentucky, Lexington, Kentucky

ABSTRACT Cardiac troponin (cTn) is a key molecule in the regulation of human cardiac muscle contraction. The N-terminal cardiac-specific peptide of the inhibitory subunit of troponin, cTnI (cTnI₁₋₃₉), is a target for phosphorylation by protein kinase A (PKA) during β -adrenergic stimulation. We recently presented evidence indicating that this peptide interacts with the inhibitory peptide (cTnI₁₃₇₋₁₄₇) when S23 and S24 are phosphorylated. The inhibitory peptide is also the target of the point mutation cTnI-R145G, which is associated with hypertrophic cardiomyopathy (HCM), a disease associated with sudden death in apparently healthy young adults. It has been shown that both phosphorylation and this mutation alter the cTnC-cTnI (C-I) interaction, which plays a crucial role in modulating contractile activation. However, little is known about the molecular-level events underlying this modulation. Here, we computationally investigated the effects of the cTnI-R145G mutation on the dynamics of cTn, cTnC Ca²⁺ handling, and the C-I interaction. Comparisons were made with the cTnI-R145G/S23D/S24D phosphomimic mutation, which has been used both experimentally and computationally to study the cTnI N-terminal specific effects of PKA phosphorylation. Additional comparisons between the phosphomimic mutations and the real phosphorylations were made. For this purpose, we ran triplicate 150 ns molecular dynamics simulations of cTnI-R145G Ca²⁺-bound cTnC₁₋₁₆₁-cTnI₁₋₁₇₂-cTnT₂₃₆₋₂₈₅, cTnI-R145G/S23D/S24D Ca²⁺-bound cTnC₁₋₁₆₁-cTnI₁₋₁₇₂-cTnT₂₃₆₋₂₈₅, and cTnI-R145G/PS23/PS24 Ca²⁺-bound cTnC₁₋₁₆₁-cTnI₁₋₁₇₂-cTnT₂₃₆₋₂₈₅, respectively. We found that the cTnI-R145G mutation did not impact the overall dynamics of cTn, but stabilized crucial Ca²⁺-coordinating interactions. However, the phosphomimic mutations increased overall cTn fluctuations and destabilized Ca²⁺ coordination. Interestingly, cTnI-R145G blunted the intrasubunit interactions between the cTnI N-terminal extension and the cTnI inhibitory peptide, which have been suggested to play a crucial role in modulating troponin function during β -adrenergic stimulation. These findings offer a molecular-level explanation for how the HCM mutation cTnI-R145G reduces the modulation of cTn by phosphorylation of S23/S24 during β -adrenergic stimulation.

INTRODUCTION

During cardiac muscle contraction, the interactions between actin and myosin are regulated by Ca²⁺ binding to troponin (cTn). Ca²⁺ binding initiates a chain of events involving structural and dynamic changes in troponin, tropomyosin, actin, and myosin, which promote cell contraction (1). The cTn protein complex consists of three subunits: troponin C (cTnC, Ca²⁺-binding subunit), troponin I (cTnI, inhibitory subunit), and troponin T (cTnT, tropomyosin-binding subunit) (2). Ca²⁺ binding to cTnC site II results in an alteration of the dynamics of the molecule, leading to a more frequent and more pronounced exposure of a hydrophobic patch on the N-terminal cTnC (NcTnC) surface between helices A and B (3). This in turn results in a greater association of the switch peptide of cTnI with the hydrophobic patch of cTnC, and a subsequent decrease in the association of cTnI with tropomyosin and actin. As a

result, tropomyosin mobility is increased and sites on actin are exposed for myosin binding (1,4,5).

The C-I interaction is critical for contractile modulation on a systolic beat-to-beat basis. During β -adrenergic stimulation, cTnI is phosphorylated by protein kinase A (PKA) at the N-terminal extension residues Ser-23 and Ser-24 (6–8). Phosphorylation at these sites reduces Ca²⁺ binding to cTn, the C-I interaction, and the Ca²⁺ sensitivity (pCa50) of force production (7–10). The cTnI N-terminal extension (NcTnI) interacts with NcTnC, which suggests that these C-I phosphorylation sites may be important in modulating C-I interactions.

Several mutations in cTnI have been associated with cardiomyopathies. In 1997, Kimura and co-workers (11) first reported that the R145G mutation in cTnI is associated with hypertrophic cardiomyopathy (HCM), the most common cause of sudden cardiac death in apparently healthy young people. Arg-145 (R145) is located in the inhibitory peptide of cTnI and thus could alter the C-I interaction and have significant effects on the function of

Submitted July 29, 2014, and accepted for publication November 21, 2014.

*Correspondence: slindert@ucsd.edu

Editor: David Sept.

© 2015 by the Biophysical Society
0006-3495/15/01/0395/13 \$2.00
<http://dx.doi.org/10.1016/j.bpj.2014.11.3461>

cTn in contraction regulation. A significant number of protein biochemical experiments have focused on analyzing the functional effects of the cTnI-R145G mutation. Initial studies reported that cTnI-R145G reduces the Ca^{2+} sensitivity of ATPase activity (12–14). Subsequent studies established that cTnI-R145G increases Ca^{2+} binding to cTn but has little effect on the exposure of the hydrophobic patch in NcTnC (15,16). However, it remains elusive how cTnI-R145G affects the C-I interaction or the structure of cTn when Ser-23 and Ser-24 are phosphorylated by PKA.

We recently investigated the effects of phosphorylation at NcTnI residues Ser-23 and Ser-24 on C-I interactions and the structure of wild-type (WT) cTn using protein biochemical and computational approaches (9,17). We also previously reported that the reduction of the C-I interaction resulting from Ser-23 and Ser-24 phosphorylation is blunted by cTnI-R145G (18). Based on previous studies (17), we speculated that cTnI-R145G interferes with the intrasubunit cTnI inhibitory peptide interaction with NcTnI to limit or abrogate the effect of PKA phosphorylation. Here, to test this hypothesis, we investigated the effects of cTnI-R145G with and without PKA phosphorylation of cTnI-S23/S24 on cTn structure and C-I interaction using molecular dynamics (MD) simulations. Previous studies have demonstrated that mutation of Ser-23 and Ser-24 to aspartic acid (S23D/S24D) results in the same changes in contractile properties of myofibrils (and trabeculae) and troponin function (in solution) as does PKA treatment of troponin (19–25). In addition, the use of these bis-phosphomimics allows one to investigate the specific role of cTnI S23/24 phosphorylation in cardiac muscle contraction, as titin and myosin binding protein C (cMyBP-C) are also phosphorylated by PKA during β -adrenergic stimulation (6,26). Thus, for this study, there are good reasons to believe that phosphomimic mutations recapitulate the effect of phosphorylation. To investigate this, we ran triplicate simulations of the core cTn complex (including residues cTnC 1–161, cTnI 1–172, and cTnT 236–285) in the cTnI-R145G state and in the cTnI-R145G/S23D/S24D state to mimic phosphorylation. Additionally, we performed triplicate simulations of the core cTn complex in the true phosphorylated state (cTnI-R145G/PS23/PS24) to compare its effects with those of the phosphomimic mutations. We found that cTnI-R145G stabilized crucial Ca^{2+} -coordinating interactions, but did not impact the overall dynamics of cTn. However, cTnI-R145G/S23D/S24D destabilized Ca^{2+} coordination and increased overall cTn fluctuations. All of the results obtained with cTnI-R145G/S23D/S24D were corroborated using the cTnI-R145G/PS23/PS24 phosphorylated system. Interestingly, cTnI-R145G also altered the intrasubunit cTnI inhibitory peptide interaction with NcTnI in a way that blunted the ability of S23/S24 phosphorylation to cause a repositioning of the N-terminal extension. These results suggest a struc-

tural basis for the blunting of PKA effects on the C-I interaction by cTnI-R145G.

MATERIALS AND METHODS

Troponin model building

We used the crystal structure of the core domain of human cTn in the Ca^{2+} -saturated form (Protein Data Bank (PDB) ID 1J1E (27)) as the basis for generating the troponin complex without the cTnI N-terminal domain. To obtain as complete a starting model as possible, we computationally rebuilt crucial residues missing in the crystal structure domains D, E, and F using physical principles and information from the PDB. Prime (28,29) was used for the cTnC modeling. Specifically, the cTnC missing residues 49 and 50 were built in and residues 35 and 84, which were mutated in the crystal structure, were modeled back to their WT state. Both the cTnI and cTnT domains had larger fragments of missing residues in the crystal structure. Therefore, we used Rosetta (30,31) to model these loop regions de novo, including the cTnI inhibitory peptide (residues 137–147) and the cTnI C-terminus (residues 192–210). The cTnI N-terminus (residues 1–39) was modeled based on the NMR structure provided by Howarth et al., as described in detail in Cheng et al. (17). The cTnT C-terminus (residues 277–288) was also added to the model. The cTnT N-terminus (residues 1–201) was not modeled, because it associates with tropomyosin (32) and does not contribute to the globular portion of cTn. The final WT cTn model contained residues cTnC 1–161, cTnI 1–210, and cTnT 202–288.

System preparation

For the simulations, we prepared three different systems of human cTn: cTnI-R145G Ca^{2+} -bound cTnC₁₋₁₆₁-cTnI₁₋₁₇₂-cTnT₂₃₆₋₂₈₅, cTnI-R145G/S23D/S24D Ca^{2+} -bound cTnC₁₋₁₆₁-cTnI₁₋₁₇₂-cTnT₂₃₆₋₂₈₅, and cTnI-R145G/PS23/PS24 Ca^{2+} -bound cTnC₁₋₁₆₁-cTnI₁₋₁₇₂-cTnT₂₃₆₋₂₈₅. The included residues were chosen to create as compact a simulation system as possible while maintaining all crucial interacting residues. Truncations were based in loop regions to fully preserve the integrity of the troponin secondary structure elements. Mutations were performed using the Mutate Residue module in VMD (33). The phosphorylations were modeled using the SP2 phosphoserine patch in VMD's psfgen. VMD was then used to add a TIP3P water box with a 14 Å padding. K^+ and Cl^- ions were added to neutralize the system and obtain a 150 mM ionic strength. The fully solvated systems contained 102,198 (cTnI-R145G Ca^{2+} -bound cTnC₁₋₁₆₁-cTnI₁₋₁₇₂-cTnT₂₃₆₋₂₈₅), 112,756 (cTnI-R145G/S23D/S24D Ca^{2+} -bound cTnC₁₋₁₆₁-cTnI₁₋₁₇₂-cTnT₂₃₆₋₂₈₅), and 112,750 (cTnI-R145G/PS23/PS24 Ca^{2+} -bound cTnC₁₋₁₆₁-cTnI₁₋₁₇₂-cTnT₂₃₆₋₂₈₅) atoms, respectively. The CHARMM27 force field (34) was used for the simulations. Two stages of minimization were performed using NAMD 2.9 (35): 10,000 steps of minimization of solvent and ions (the protein was restrained using a force constant of 500 kcal/mol/Å²) followed by a 10,000 step minimization of the entire system without any restraints. A short initial 380 ps MD simulation with consecutively weaker restraints (10–0.1 kcal/mol/Å²) on the protein residues was used to heat up the system to a temperature of 300 K. The equilibration was finished by a short 20 ps NPT simulation without any restraints.

MD simulations

All simulations were performed under the NPT ensemble at 300 K using NAMD 2.9 (35) and the CHARMM27 force field (34). Periodic boundary conditions were used along with a nonbonded interaction cutoff of 12 Å. Bonds involving hydrogen atoms were constrained using the SHAKE algorithm (36), allowing for a time step of 2 fs. Structures were saved every 2 ps. Triplicate 150 ns MD simulations (three independent 150 ns simulations) were performed on all systems, and each simulation of the same system started from different conformations of the cTnI N-terminal extension.

Contact analysis

The residue-residue contacts between cTnC and key regions of cTnI (N-terminus, inhibitory peptide, and switch peptide regions), as well as intrasubunit contacts between the cTnI N-terminus and inhibitory peptide, were monitored over the course of all simulations. Contacts between NcTnC-NcTnI, the NcTnC-switch peptide of cTnI, and the cTnC-inhibitory peptide of cTnI were monitored. The intrasubunit interaction between the N-terminus and the inhibitory peptide region of cTnI were also recorded. Contacts between two residues were defined as previously described by Wang et al. (37), with a carbon-carbon distance of ≤ 5.4 Å and a distance between any other noncarbon atoms of ≤ 4.6 Å being defined as a contact. For each residue contact pair, the fraction of the simulation time in which these residues were in contact was calculated for the two simulation systems.

Calcium coordination

To monitor the stability of the coordination between the calcium ion and its cTnC site II binding residues, we recorded the time evolution of the following distances: Ca²⁺-Asp-65 OD2, Ca²⁺-Asp-67 OD2, Ca²⁺-Ser-69 OG, Ca²⁺-Thr-71 OG1, Ca²⁺-Asp-73 OD2, and Ca²⁺-Glu-76 OE2. These atoms correspond to the atoms that Ca²⁺ coordinates within the crystal structure. Since the Ca²⁺ coordination atoms within a residue occasionally switched during the course of the simulations, we also recorded distances between the following possible alternate coordinating atoms: Ca²⁺-Asp-65 OD1, Ca²⁺-Asp-67 OD1, Ca²⁺-Asp-73 OD1, and Ca²⁺-Glu-76 OE1. Residues Ser-69 and Thr-71 do not have possible alternative coordinating atoms. Distances in the WT Ca²⁺-bound cTnC₁₋₁₆₁-cTnI₁₋₁₇₂-cTnT₂₃₆₋₂₈₅ (17), cTnI-R145G Ca²⁺-bound cTnC₁₋₁₆₁-cTnI₁₋₁₇₂-cTnT₂₃₆₋₂₈₅, and cTnI-R145G/S23D/S24D Ca²⁺-bound cTnC₁₋₁₆₁-cTnI₁₋₁₇₂-cTnT₂₃₆₋₂₈₅ systems were measured every 2 ps. For the sake of analysis, the minimum distances between Ca²⁺ and the coordinating atom on each residue were plotted.

Molecular mechanics/generalized Born surface area analysis

Molecular mechanics/generalized Born surface area (MM/GBSA) (38) analysis was used to score cTnI/cTnC binding interactions. The free energy of binding for the MM/GBSA method is defined as

$$G = E_{\text{tot}} - T S, \quad (1)$$

where G , E_{tot} , and S are the free energy, total enthalpy, and total entropy, respectively, and T is the system temperature. In this study, we assumed that the solute contributions to the entropy were comparable among the cTnI mutants; thus, we estimated the free energy as

$$G = G_{\text{solvation}} + E_{\text{VDW}} + E_{\text{INT}}, \quad (2)$$

where $G_{\text{solvation}}$ is the solvation free energy, E_{VDW} is the van der Waals energetic contribution, while E_{INT} corresponds to internal energies arising from bonds, angles and dihedrals at 0 K. These terms were evaluated using the NAMD simulation engine (35) and the CHARMM 27 force field (34), using the parameters defined above, as well as the gbs keyword for the GB calculation at an ionic strength of 0.15 M. MM/GBSA was applied to snapshots recorded at 1 ns intervals from each WT, cTnI-R145G, and cTnI-R145G/S23D/S24D protein simulation. The binding score, $\Delta G^{\text{Binding}}$, was estimated by

$$\Delta G^{\text{Binding}} = G_{\text{TnC/TnI}} - G_{\text{TnI}} - G_{\text{TnC}}, \quad (3)$$

where $G_{\text{TnC/TnI}}$ is the energy of the TnC/TnI complex, and G_{TnI} and G_{TnC} correspond to the energies of the isolated cTnI and cTnC components,

respectively. The solvation free energy was computed as the sum of electrostatic and nonpolar contributions (39)

$$G_{\text{solvation}} = G_{\text{electrostatic}} + G_{\text{nonpolar}}. \quad (4)$$

To estimate $G_{\text{electrostatic}}$, we utilized the GB approximation to the Poisson-Boltzmann equation, the latter of which quantifies the electrostatic contribution of fixed charges within a solute immersed in an electrolyte solution (40). The NAMD GB implementation (41) is based on an approximation for the Born radii proposed originally by Onufriev et al. (42) for numerical stability. The authors reported agreement between GB and PB within 2–5 kcal/mol for two model protein systems, which we expected was reasonably accurate for our estimates. The nonpolar term, G_{nonpolar} , was calculated in NAMD as a function of the solvent-accessible surface area (SASA) (43) using

$$G_{\text{nonpolar}} = \text{SASA} \cdot \gamma, \quad (5)$$

where the SASA was computed via the LCPO method (44) and $\gamma = 0.0072$ kcal/mol/Å² (45) in accordance with related studies on protein-protein complexes (46).

RESULTS AND DISCUSSION

cTnI-R145G has little impact on fluctuations of the cTn structure

The WT cTn model on which all of the simulations were based is shown in Fig. 1, with the side chains of cTnI residues S23, S24, and R145 highlighted to identify their positions. cTnI-R145G and cTnI-R145G/S23D/S24D mutant systems were generated by introducing the corresponding mutations into this model. The cTnI-R145G/PS23/PS24 system was generated by introducing the cTnI-R145G and replacing cTnI-S23 and cTnI-S24 with phosphoserine residues. Fig. S1 in the Supporting Material shows the root mean-square deviation (RMSD) versus time plots for the cTnI-R145G, cTnI-R145G/S23D/S24D, and cTnI-R145G/PS23/PS24 cTn simulations. All systems reached an equilibrated state within the simulation time of

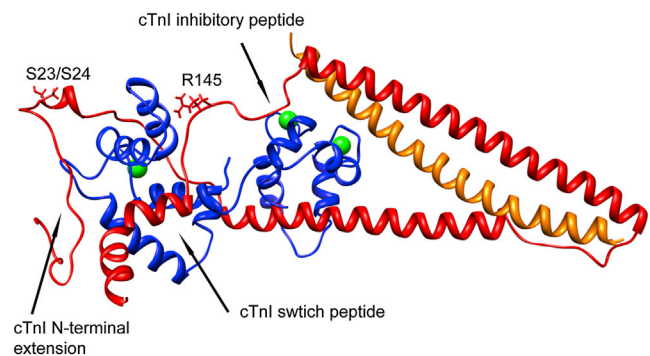


FIGURE 1 Static snapshot of the initial structures of the cTn complex built up based on the PDB 1J1E crystal structure and Howarth et al.'s NMR structure including the N-terminal extension. cTnC (residues 1–161) is shown in blue, cTnI (residues 1–171) is in red, and cTnT (residues 236–285) is in orange. The mutational site cTnI-R145 and the two PKA phosphorylation sites (cTnI-S23/S24) are shown in stick representation.

150 ns. Our first goal was to assess the effect of cTnI-R145G on the dynamics of the cTn protein complex. To compare the dynamics of WT versus cTnI-R145G cTn, we performed triplicate MD simulations and calculated the average root mean-square fluctuation (RMSF, \pm SD) values for all residues. Fig. 2 shows the RMSF of the cTnC and cTnI subunits for the WT and the cTnI-R145G system. Interestingly, the fluctuations in the cTnI-R145G mutant system were comparable to those in the WT system throughout most of the protein structure (average RMSFs of 2.8 Å and 2.9 Å, respectively). The only pronounced difference was seen in the C-terminal domain of cTnC (cTnC

residues 120–130), the loop connecting the two C-terminal cTnC EF-hand motifs (which interacts with the cTnI I-T arm), although a small difference may also exist in the linker region connecting the N- and C-terminal lobes of cTnC (cTnC residues 80–100). Most of the other regions did not exhibit changes larger than the standard deviations (SDs). The largest fluctuations were observed in the NcTnI region, underscoring its highly flexible nature. The first 20 cTnI residues were the most flexible, and cTnI_{20–40} showed a lower degree of flexibility—a trend that was also observed in a recent NMR study by Hwang et al. (47). With fluctuations this large, it is appropriate to refer to a range of conformations for NcTnI rather than an actual single structural conformation. The helical bundle known as the IT arm (cTnI residues 42–80 and 100–137) comprised the most stable residues in the cTnI subunits, reflecting their structural rather than regulatory function. Fig. 2 A also highlights regions of cTn that play an important part in either Ca²⁺ binding (cTnC site I and cTnC site II) or the C-I interaction. In contrast to previous studies on WT and phosphomimic WT cTn (or cTnI-S23D/S24D cTn) (17), we found that the fluctuations in all of these regions were not influenced by cTnI-R145G. In summary, cTnI-R145G had little impact on the dynamics of the troponin complex. This can also be seen in Fig. 2, B and C, where eight 20 ns incremental simulation snapshots for the WT and cTnI-R145G mutation simulations are superimposed. These findings suggest that the predominant mechanism of enhanced Ca²⁺ binding and C-I interaction by cTnI-R145G is not the overall structural fluctuations, at least on the timescale accessible to our MD simulations. Our full-atom cTn model is a great complement to the thin-filament model proposed by Manning et al. (32,48). The cTn model is a good tool for examining detailed molecular interactions and obtaining measures of rapid kinetic dynamics, whereas the cTn-Tm thin-filament model provides an excellent picture of the long-range consequences of local altered structure.

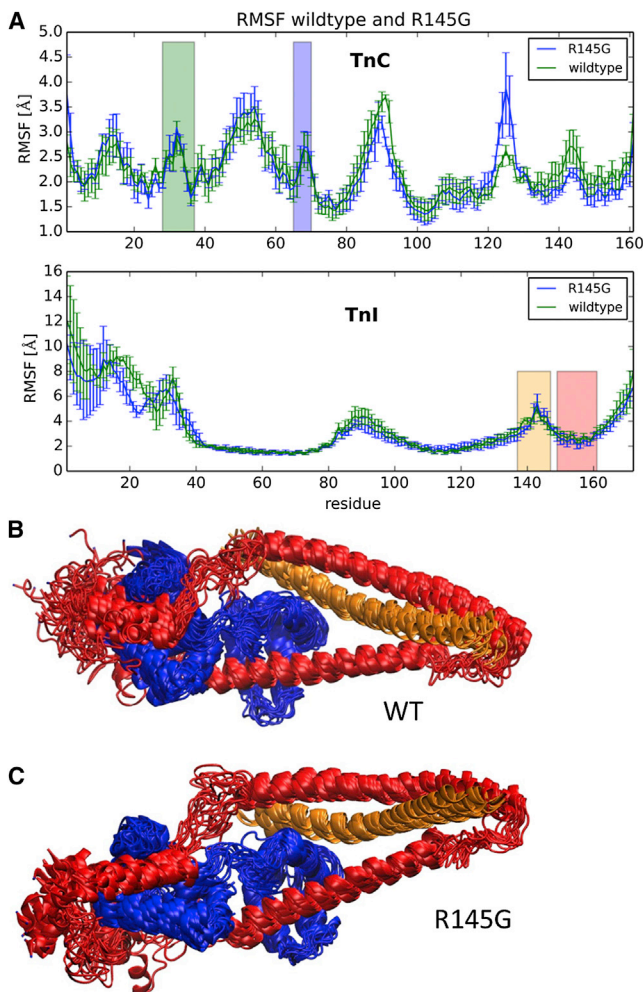


FIGURE 2 (A) Comparison of RMSF values of the simulations of WT (green) and cTnI-R145 (blue) troponin. Shaded boxes indicate important regions in the protein: the cTnC (inactive) calcium binding site I (green), the cTnC calcium binding site II (blue), the cTnI inhibitory peptide (yellow), and the cTnI switch peptide (red). Uncertainties in RMSF values were determined by running three independent 150 ns MD simulations and are given as error bars on the plots. (B and C) Ribbon representations of the conformations assumed by the troponin molecule during (B) the WT simulation and (C) the cTnI-R145 mutation simulation. cTnC is shown in blue, cTnI is in red, and cTnT is in gold. Molecular simulation snapshots recorded every 20 ns are shown.

Phosphomimic mutations and phosphorylation of S23 and S24 in cTnI-R145G result in increased fluctuations throughout the cTn structure

Next, we investigated the influence of PKA phosphorylation on cTn containing cTnI-R145G. For this purpose, we performed simulations with simultaneous phosphomimic mutations S23D and S24D and cTnI-R145G in the troponin structure. Fig. 3 shows the RMSF of the cTnC and cTnI subunits for the cTnI-R145G and cTnI-R145G/S23D/S24D system. The fluctuations in the cTnI-R145G/S23D/S24D mutant system (average RMSF 3.2 Å) were increased with respect to the cTnI-R145G system (average RMSF 2.8 Å), akin to what we previously reported for WT and cTnI-S23D/S24D simulations (17). This increased fluctuation may precipitate the increased fluctuations seen in

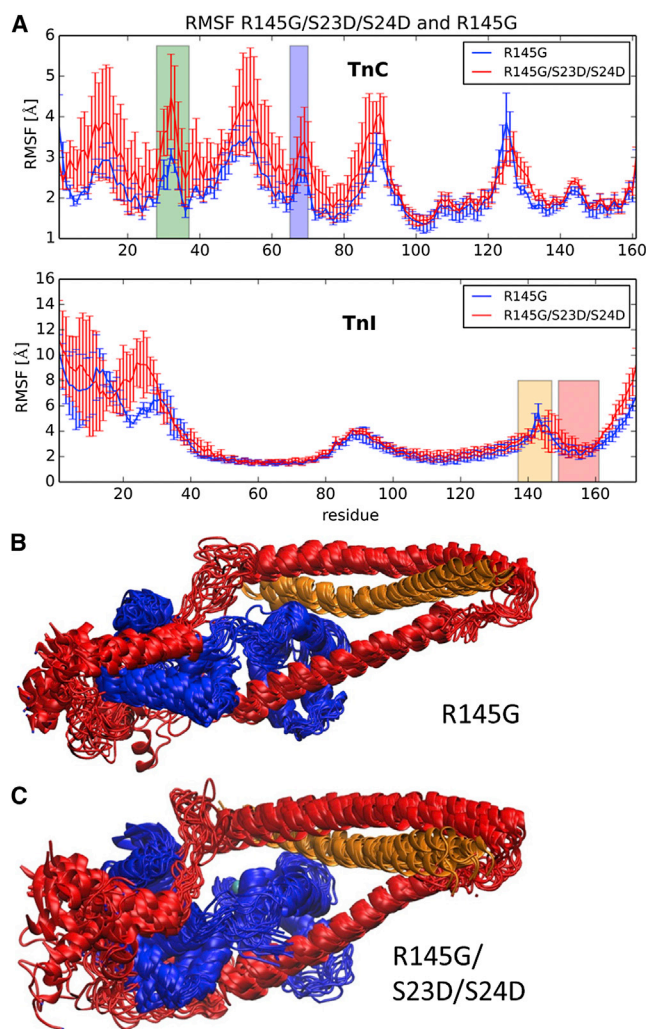


FIGURE 3 (A) Comparison of RMSF values of the simulations of cTnI-R145 (blue) and cTnI-R145G/S23D/S24D (red) troponin. Shaded boxes indicate important regions in the protein: the cTnC (inactive) calcium binding site I (green), the cTnC calcium binding site II (blue), the cTnI inhibitory peptide (yellow), and the cTnI switch peptide (red). Uncertainties in RMSF values were determined by running three independent simulations and are given as error bars on the plots. (B and C) Ribbon representations of the conformations assumed by the troponin molecule during (B) the cTnI-R145 mutation simulation and (C) the cTnI-R145G/S23D/S24D simulation. cTnC is shown in blue, cTnI is in red, and cTnT is in gold. Molecular simulation snapshots recorded every 20 ns are shown.

NcTnC (Fig. 3 A, top, residues 1–89). Interestingly, there were increased dynamics in the entire structure of NcTnC, suggesting that NcTnI mobility can have a profound influence on NcTnC structure. The average RMSF for the cTnC site I increased from 2.6 Å in the cTnI-R145G system to 3.6 Å in the cTnI-R145G/S23D/S24D system, an increase beyond the SD of the triplicate simulations. The cTnC site II had an RMSF of 2.8 Å in the cTnI-R145G system, compared with 3.5 Å in the cTnI-R145G/S23D/S24D system. The increased RMSF of site II may be related to a destabilization of Ca^{2+} in the site II binding pocket of

cTnC, leading to the increase in Ca^{2+} dissociation rate that has been reported for cTn following phosphorylation by PKA (16,49). No significant change in fluctuations was observed in the inhibitory peptide or the switch peptide of cTnI, suggesting that their interaction with NcTnC is not affected. The significance of this is discussed further below. Fig. 3 C shows snapshots of the cTnI-R145G/S23D/S24D system simulations. The increased cTnC (blue) flexibility for the cTnI-R145G/S23D/S24D system compared with cTnI-R145G (Fig. 3 B) is demonstrated by the cTn snapshots. The largest change in dynamical behavior between the two systems occurred in cTnI residues 20–30 (not visible in the snapshot structures), where a statistically significant increase in local residue fluctuations was observed. The Ser (S) to Asp (D) mutations broke, stabilizing interactions in the region (shown in detail further below). In the cTnI-R145G system (with no phosphomimetic mutations), this region was the most stable part of NcTnI. Upon introduction of phosphomimetic mutations, RMSF values as high as 9–10 Å were observed (compared with 4–5 Å for the cTnI-R145G system), suggesting a large increase in the mobility of NcTnI. Simulating the actual phosphorylated cTn system allowed us to compare the effects of phosphomimetic mutations with those due to the presence of real phosphoserine residues. To that end, we performed simulations with phosphoserine substitutions at residues cTnI-S23 (cTnI-PS23) and cTnI-S24 (cTnI-PS24) and the cTnI-R145G mutation in the troponin structure. Fig. S2 shows the RMSF of the cTnC and cTnI subunits for the cTnI-R145G/S23D/S24D and cTnI-R145G/PS23/PS24 systems. The overall fluctuations in both systems are virtually indistinguishable, supporting the use of phosphomimetic mutations instead of phosphoserine residues. A noticeable difference can be found within NcTnI; however, even there, the two systems agree within the error bars.

MM/GBSA assessment of cTnC/cTnI binding interactions

MM/GBSA (38) analysis was used to qualitatively estimate the binding affinity of the cTnI switch peptide to NcTnC. Although methods such as thermodynamic integration can provide binding free-energy estimates that are in comparatively better agreement with experiments, they do so at a computational cost that is intractable for large systems, such as the cTn used in this study. MM/GBSA estimates the internal energy of a solute using an all-atom, explicit molecular force field while treating all solute/solvent interactions implicitly through the GB level of solvation theory (38). MM/GBSA has shown promise for rank-ordering protein-protein binding free energies (39,50), as well as cTnC/cTnI binding (51), although quantitative agreement is still lacking (52). Therefore, we consider the MM/GBSA scores here as scores to indicate their predictive power in ranking

ligands, as opposed to providing quantitative agreement with experimentally observed affinities.

In Fig. 4, we report the means and confidence intervals of the MM/GBSA binding scores for the cTnC/cTnI interface (cTnC residues 1–90, cTnI residues 138–171) for the WT, cTnI-R145G, and cTnI-R145G/S23D/S24D protein systems, based on the three independent MD simulation runs for each cTnI configuration. In our application of MM/GBSA, we neglect entropic contributions of the solute to the free energy, which are known to be important (but difficult to compute) contributors to protein stability and substrate binding (53). For each simulation, MM/GBSA analysis was applied to 15 snapshots recorded at 1 ns intervals. The means for each simulation are reported along with the 95% confidence interval based on the standard error of the means for each independent simulation. We find that the mean binding score is more favorable for the cTnI-R145G systems relative to the WT. The mean score for the cTnI-R145G/S23D/S24D case appears to be comparable to that for cTnI-R145G, but still greater than the WT mean affinity. Thus, these scores suggest that the contacts formed between the cTnC/cTnI complex containing cTnI-R145G relative to the WT are more energetically favorable, whereas the phosphomimics cTnI-R145G/S23D/S24D contacts are negligibly different from the nonphosphomimic. Our findings are in qualitative agreement with experimental trends that we recently reported, in which the strength of cTnC/cTnI affinities were ordered as cTnI-R145G > cTnI-R145G/S23D/S24D > WT, respectively (18). In so far as stronger C-I binding is correlated with enhanced Ca²⁺ affinity, our predictions may in part explain 1), the left-shifted Ca²⁺ sensitivity of force generation and prolonged initial phase (slow phase) of relaxation for cTnI-R145G relative to the WT (54); and 2), the insensitivity

of Ca²⁺-dependent myosin ATPase activity to PKA phosphorylation of cTnI-R145G relative to the WT (12).

Calcium coordination

Previous solution biochemical measurements demonstrated an increased binding affinity of Ca²⁺ to cTn containing cTnI-R145G compared with WT cTnI (16). However, upon PKA phosphorylation, there is a decrease in Ca²⁺ binding affinity for cTn containing either cTnI-R145G or WT (9). Thus, it is reasonable to hypothesize that the cTnI-R145G mutation and PKA phosphorylation may both impact Ca²⁺ binding stability in site II. Due to the nature of divalent cations, it is very difficult to calculate the binding affinities of Ca²⁺ accurately. Therefore, we investigated one measure related to Ca²⁺ binding in site II in cTnC: the time evolution of distances between the bound Ca²⁺ ion and its coordinating residues. In the crystal structures, Ca²⁺ is coordinated with six atoms in cTnC site II residues: Asp-65 OD2, Asp-67 OD2, Ser-69 OG, Asp-73 OD2, Glu-76 OE1, and Glu-76 OE2. As observed in previous studies (17), the coordinating behavior of Asp-65, Asp-67, Asp-73, and Glu-76 did not change for WT cTn in the absence or presence of cTnI-S23D/S24D. Data for the cTnI-R145G and cTnI-R145G/S23D/S24D cTn simulations are shown in Fig. S3. The most interesting behavior was observed for Ser-69 OG and, perhaps, Thr-71 OG1. Fig. 5 shows those distances over the course of the three independent 150 ns simulations for WT, cTnI-R145G, and cTnI-R145G/S23D/S24D cTn systems. The coordination behavior for both residues fluctuated over the course of the simulations for all three systems, in contrast to the stability of the other four coordinating residues (Fig. S3). Thr-71 generally did not coordinate, in agreement with structural data from x-ray crystallography. The most pronounced difference between the simulations was observed in coordination of Ser-69. As demonstrated in Fig. 5, Ser-69 was the most flexible of all the coordinating residues, which is consistent with previous findings (17,37,55). However, the percent-in-contact time of Ser-69 varied among the different systems. Whereas Ser-69 was coordinating for ~10% of the total cumulative simulation time of 450 ns in the WT system, this fraction increased to 29% in the cTnI-R145G system, indicating a stronger interaction and a possible stabilization. This may suggest how the Ca²⁺ binding affinity is increased for cTn containing cTnI-R145G, in agreement with previous studies on cTnC mutations in which Ca²⁺ binding at site II was stabilized (37). Interestingly, the contact time was decreased to 6% upon introduction of the phosphomimic mutation (cTnI-R145G/S23D/S24D mutant system), in agreement with a reduction in Ca²⁺ binding affinity seen in previous solution studies (18). Together, these experimental and simulation data suggest that Ser-69 may be a critical coordinating position for conferring the Ca²⁺ binding affinity of site II in cTn.

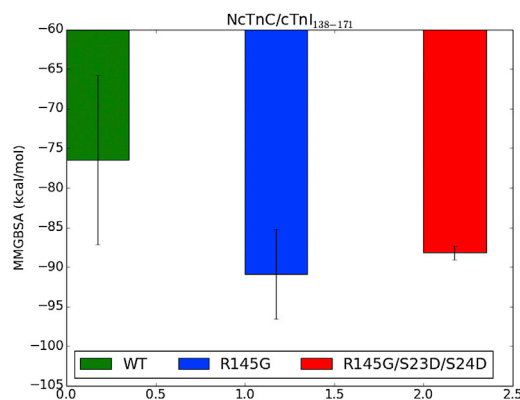


FIGURE 4 MM/GBSA analysis applied to the cTnC/cTnI interface (cTnC residues 1–90, cTnI residues 138–171) using 150 snapshots recorded at 1 ns intervals for WT (green), cTnI-R145G (blue), and cTnI-R145G/S23D/S24D (red) cTn complexes. Each bar represents the mean from three independent simulations, and error bars represent the 95% confidence interval. To see this figure in color, go online.

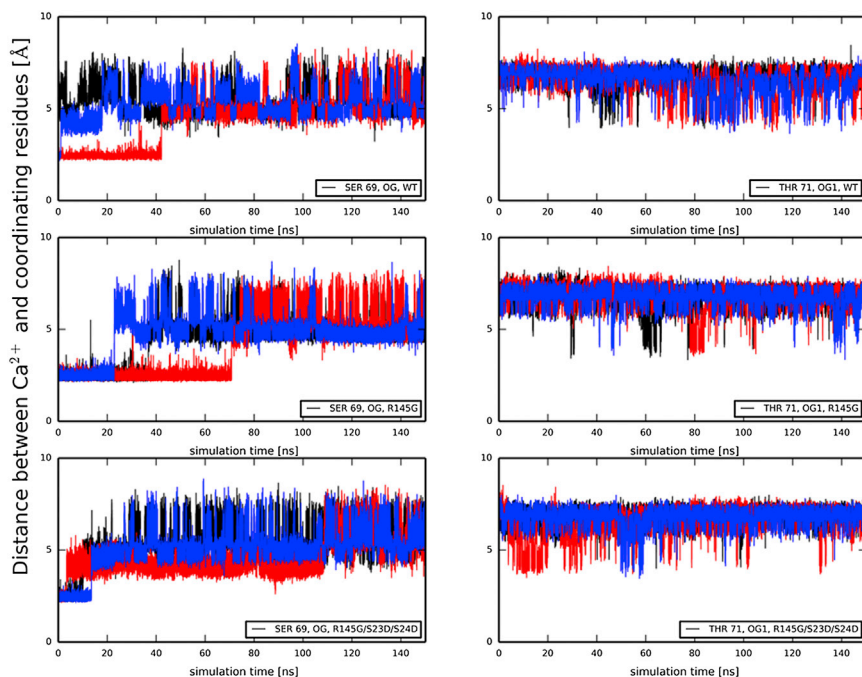


FIGURE 5 Distances between Ca^{2+} and two coordinating cTnC site II atoms Ser-69 OG (*left*) and Thr 71 OG1 (*right*) over the course of the MD simulations for the WT (top), the cTnI-R145G system (*center*), and the cTnI-R145G/S23D/S24D mutant system (*bottom*). Results for the three independent simulations (simulation 1 (*black*), simulation 2 (*red*), and simulation 3 (*blue*)) are overlaid in the plots. To see this figure in color, go online.

Contact analysis identifies hotspot residue contact pairs that are most affected by introduction of the cTnI-R145G and bis-phosphomimic mutations

In the troponin complex, the C-I interaction is a critical point in the Ca^{2+} activation of contraction, and thus it makes sense to consider this as a point of modulation during β -adrenergic stimulation. There are three regions of contacts that are of particular interest: 1), C-I contacts between the switch and inhibitory peptides and the cTnC molecule; 2), C-I contacts between the cTnI N-terminal extension and the cTnC molecule; and 3), intrasubunit cTnI contacts between the cTnI N-terminal extension and the inhibitory peptide. In a previous study, we elucidated these contacts for the WT and cTnI-S23D/S24D cTn systems (17). Here, we performed a contact analysis of the cTnI-R145G and cTnI-R145G/S23D/S24D cTn systems.

cTnI switch peptide-NcTnC and cTnI inhibitory peptide-cTnC interactions

First, we analyzed contacts between the cTnI switch peptide (cTnI residues 148–164) and NcTnC (cTnC residues 1–89), and between the cTnI inhibitory peptide (cTnI residues 138–147) and cTnC. The results are shown in Fig. S4 (comparison of cTnI-R145G with WT) and Fig. 6 (comparison of cTnI-R145G with cTnI-R145G/S23D/S24D). Additionally, Fig. S5 shows a similar comparison with respect to the phosphorylation simulations (comparison of cTnI-R145G with cTnI-R145G/PS23/PS24). Average contact maps for interactions between the cTnI switch peptide

and NcTnC are shown in panels A (cTnI-R145G model) and C (WT or the cTnI-R145G/S23D/S24D or cTnI-R145G/PS23/PS24 model, respectively). The blue end of the spectrum (value = 0) reflects no contact between a residue-residue pair during the total cumulative simulation time of 450 ns, and the red end of the spectrum (value = 1) represents 100% contact time between a residue-residue pair. Contact patterns reminiscent of the WT systems, where cTnC helices A, B, and D interact with the cTnI switch peptide, are observed. There is no dramatic change in the contact pattern of the switch peptide residues due to either introduction of cTnI-R145G or subsequent phosphomimic mutations (as well as phosphorylation of S23 and S24), as can be seen in the difference contact map for panels A and C (Figs. 6 E, S4 E, and S5 E). In this map, the color green (value = 0) reflects no difference between the two systems, the red end of the spectrum (values > 0) reflects more contacts in the cTnI-R145G cTn system, and the blue of the spectrum (values < 0) indicates more contacts in the WT or cTnI-R145G/S23D/S24D or cTnI-R145G/PS23/PS24 model, respectively. The right-hand side panels in Figs. 6, S4, and S5 (panels B and D) show the contacts between cTnI inhibitory peptide and cTnC. The inhibitory peptide interacts with two main regions of cTnC: the cTnC helix C and the linker between the N- and C-terminal lobes of cTnC. The difference contact maps indicate that R145 breaks most of the contacts it has formed upon mutation to glycine (Fig. S4 F). Fig. 6 F also indicates that more stable interactions between the inhibitory peptide and its interacting regions are formed as a consequence of phosphomimic mutations. This is

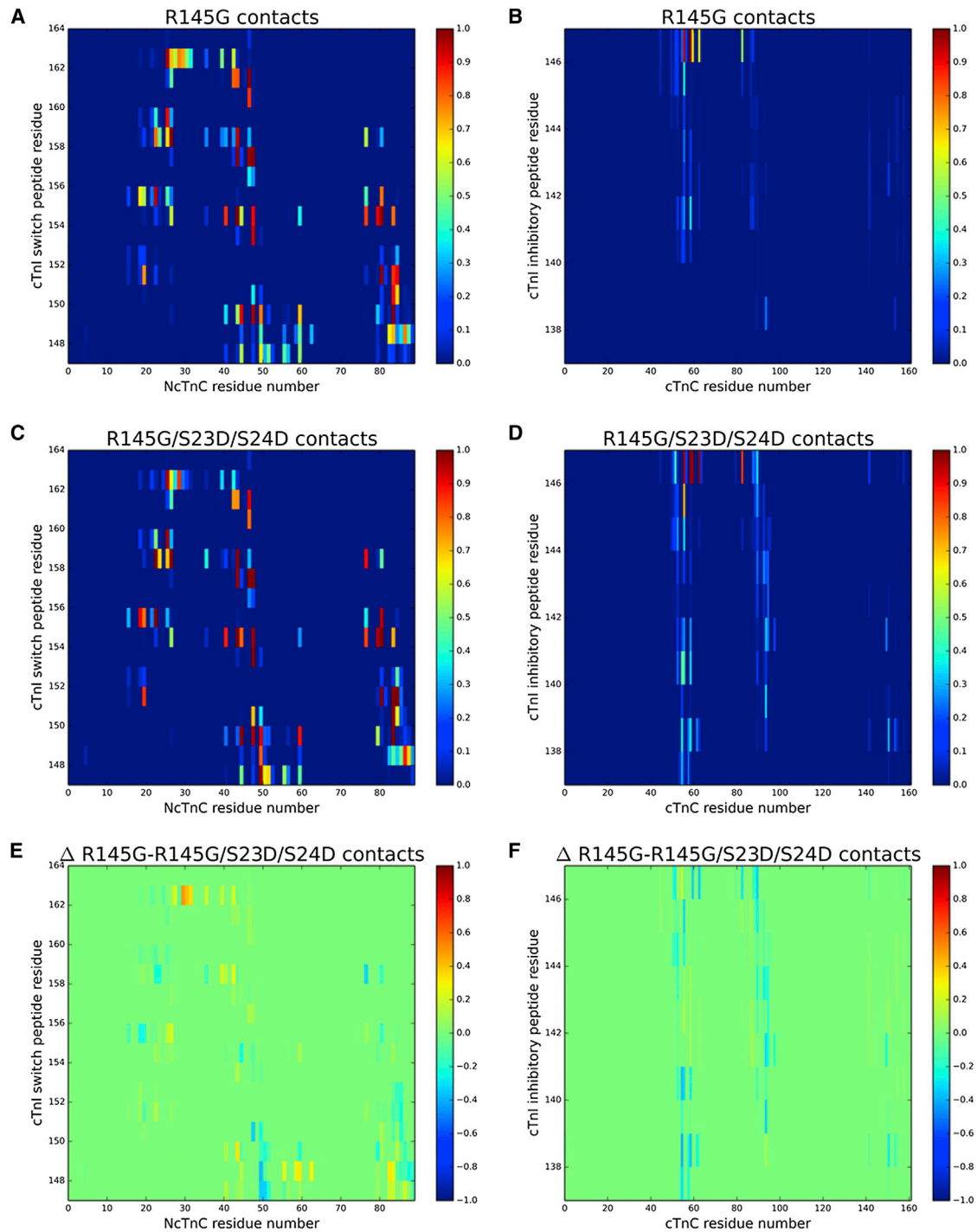


FIGURE 6 (A and C) Average contact maps of residue-residue pairs between NcTnC (cTnC residues 1–89) and cTnI switch peptide (cTnI residues 148–164) for (A) cTnI-R145G and (C) cTnI-R145G/S23D/S24D complexes. (B and D) Average contact maps of residue-residue pairs between cTnC and cTnI inhibitory peptide (cTnI residues 138–147) for (B) cTnI-R145G and (D) cTnI-R145G/S23D/S24D complexes. (E) Difference contact map of residue-residue pairs between NcTnC and cTnI switch peptide that were most affected by introduction of the phosphomimic mutations. (F) Difference contact map of residue-residue pairs between cTnC and cTnI inhibitory peptide that were most affected by introduction of phosphomimic mutations. (E and F) In the difference contact maps, values > 0 (yellow and red) correspond to two residues that are more frequently in contact in the cTnI-R145G simulation compared with the cTnI-R145G/S23D/S24D simulation. Values < 0 (blue) correspond to two residues that are more frequently in contact in the cTnI-R145G/S23D/S24D simulation compared with the cTnI-R145G simulation.

indicative of a stabilization of the cTnI inhibitory peptide upon phosphorylation. This effect is mirrored in the simulations of the real phosphorylations, as can be seen in Fig. S5 F.

NcTnI-NcTnC interactions

Second, we analyzed contacts between NcTnI (cTnI residues 1–41) and NcTnC (cTnC residues 1–89). The results are shown in Fig. S6 (comparison of cTnI-R145G with WT) and Fig. 7 (comparison of cTnI-R145G with cTnI-R145G/S23D/S24D). Additionally, Fig. S7 shows a similar comparison with respect to the phosphorylation simulations (comparison of cTnI-R145G with cTnI-R145G/PS23/PS24). Average contact maps are shown in panels A (cTnI-R145G model) and B (WT or cTnI-R145G/S23D/S24D or cTnI-R145G/PS23/PS24 model). The blue end of the spectrum (value = 0) reflects no contact between a residue-residue pair during the total cumulative simulation time of 450 ns, and the red end of the spectrum (value = 1) represents 100% contact time between a residue-residue

pair. Most of the interactions involved two cTnC regions: the loop between helices A and B (site I) and the site II Ca^{2+} binding site. The introduction of cTnI-R145G changed the general contact pattern and maintained contacts with site I and site II (see Fig. S6). Interestingly, all interaction hotspots also remained after introduction of either the S23D/S24D mutations (see Fig. 7) or the PS23/PS24 phosphorylations (see Fig. S7). This is in contrast to the behavior observed for the WT system (17), where contacts between NcTnI and the loop between cTnC helices A and B were completely lost upon introduction of the phosphomimic mutations. Loss of contacts was associated with a large-scale repositioning of the NcTnI peptide to form stable interactions with the cTnI inhibitory peptide, which we hypothesized to be a crucial molecular consequence of phosphorylation (17). To our knowledge, this is the first indication that cTnI-R145G alters the behavior of cTn upon phosphorylation. Again, this effect was observed in both the phosphomimic and phosphorylated systems.

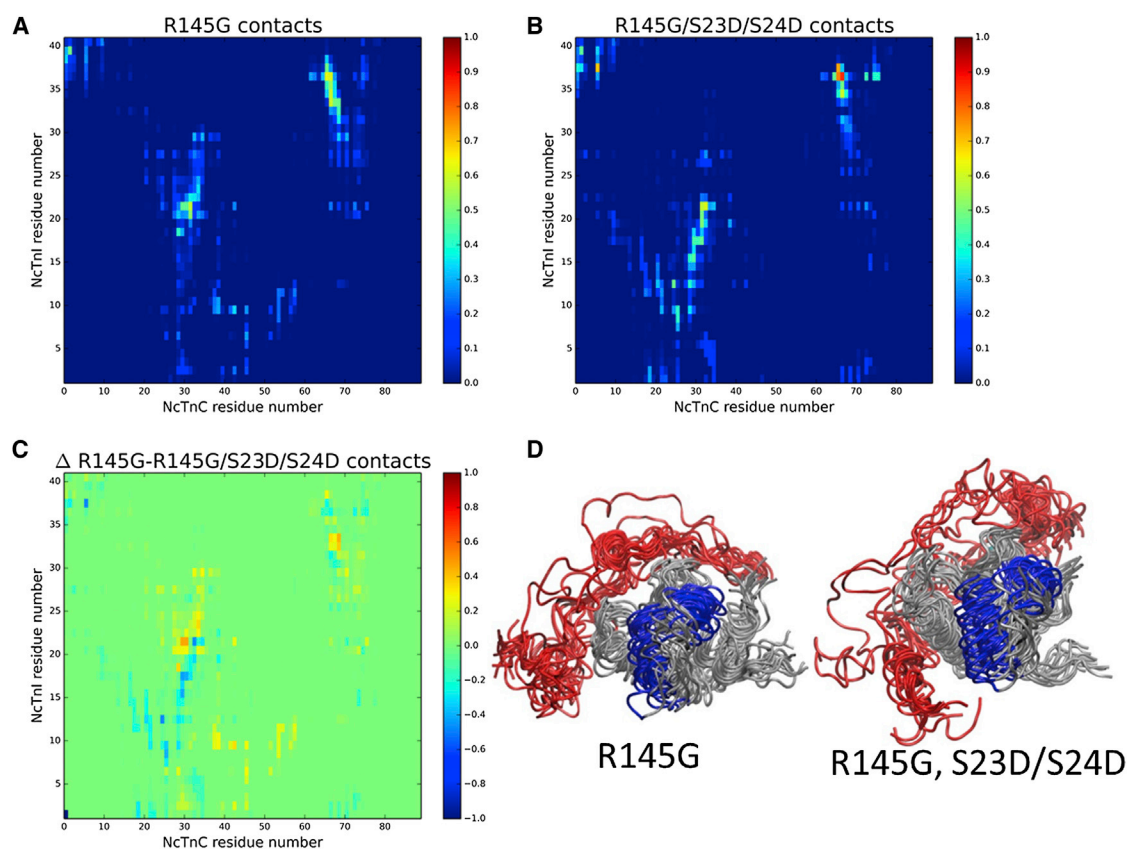


FIGURE 7 (A and B) Average contact map of residue-residue pairs between NcTnC (cTnC residues 1–89) and NcTnI (cTnI residues 1–41) for (A) cTnI-R145G and (B) cTnI-R145G/S23D/S24D complexes. (C) Difference contact map of residue-residue pairs between NcTnC and NcTnI that were most affected by introduction of the phosphomimic mutations. Values > 0 (yellow and red) correspond to two residues that are more frequently in contact in the cTnI-R145G simulation compared with the cTnI-R145G/S23D/S24D simulation. Values < 0 (blue) correspond to two residues that are more frequently in contact in the cTnI-R145G/S23D/S24D simulation compared with the cTnI-R145G simulation. (D) Comparison of interactions between NcTnC and NcTnI during the last 70 ns (from 80 ns to 150 ns) MD simulations for cTnI-R145G and cTnI-R145G/S23D/S24D complexes. The NcTnC (residues 1–89) is shown in gray, the B-helix (residues 38–48) and C-helix (residues 54–64) are in blue, and NcTnI (residues 1–41) is in red.

Intrasubunit cTnI inhibitory peptide-NcTnI Interactions

It was previously shown both experimentally and computationally that bisphosphorylation at S23/S24 of the N-terminal residues in cTnI or mutation of these positions to Asp results in a weakened interaction with NcTnC residues (56,57). It was also shown that the cTnI N-terminal residues are repositioned to form favorable interactions with basic regions of cTnI, such as the inhibitory region of cTnI (17,56). This constitutes an important mechanism by which PKA can regulate cTn structure and dynamics. An interesting question arises: to what degree does the HCM mutation cTnI-R145G impact this mechanism? We hypothesized that cTnI-R145G dramatically disrupts this mechanism to blunt the ability of PKA regulation. To investigate this, we elucidated intrasubunit contacts between NcTnI (cTnI residues 1–41) and the cTnI inhibitory peptide (cTnI residues 138–147). Fig. 8 shows the corresponding contact plots for (A) WT, (B) cTnI-R145G, (C) cTnI-S23D/S24D, (D) cTnI-R145G/S23D/S24D, and (E) cTnI-R145G/PS23/PS24 cTn complexes. As was previously observed (17), there were no interactions between the cTnI inhibitory peptide and NcTnI in the WT cTn system (Fig. 8 A). However, this changed dramatically upon introduction of the cTnI-S23D/S24D mutations (Fig. 8 C): all three independent runs formed contacts between cTnI residues 9–14 and 140–142 for ~50% of the simulation time (Fig. 8 C). No intrasubunit interactions were seen in the cTnI-R145G system (Fig. 8 B), which is not surprising since no phosphomimetic mutations or phosphorylations were present. However, introduction of the cTnI-R145G mutation also blunted all NcTnI-cTnI inhibitory peptide interactions in the phosphomimetic system (cTnI-R145G/S23D/S24D; Fig. 8 D) as well as the phosphorylated system (cTnI-R145G/PS23/PS24; Fig. 8 E). Introduction of the glycine in the cTnI R145 inhibitory peptide residue may change the structural dynamics of the cTnI inhibitory peptide in a way that interferes with its interaction with NcTnI. This suggests that a possible mechanism of action of the cTnI-R145G mutation is interference with PKA regulation. We speculate that the intracTnI contacts increase the stability of the inhibitory/switch peptide region with NcTnC, which may explain the increased C-I affinity in the presence of the cTnI-R145G mutation (18). PKA phosphorylation speeds the early phase of relaxation, possibly resulting from the altered NcTnI-cTnI inhibitory peptide interactions in the presence of the cTnI-R145G mutation.

CONCLUSIONS

Computational methods can play an important role in elucidating the molecular underpinnings of mutational effects on protein structure, dynamics, and function. Here, we used MD simulations to investigate the effects of a mu-

tation of the inhibitory subunit of human cTn. cTnI-R145G is associated with HCM, a vicious genetic heart muscle disease that causes sudden death in otherwise healthy young adults. Additionally, we investigated the combined effects of cTnI-R145G and phosphorylation by PKA during β -adrenergic stimulation through both cTnI-R145G/S23D/S24D phosphomimics and cTnI-R145G/PS23/PS24 phosphorylations. In summary, we found that cTnI-R145G stabilized crucial Ca^{2+} -coordinating interactions without changing the overall cTn dynamics. On the other hand, cTnI-R145G/S23D/S24D destabilized Ca^{2+} coordination and increased overall cTn fluctuations. Most notably, cTnI-R145G also altered the intrasubunit cTnI inhibitory peptide interaction with NcTnI in a way that blunted the ability of PKA phosphorylation to cause a repositioning of the N-terminal extension. These results suggest a structural basis for the blunting of PKA effects on the C-I interaction by cTnI-R145G. Furthermore, we performed a vigorous comparison of effects caused by phosphomimetic mutations versus phosphorylated serines. All of the results presented here were independent of the system used, which suggests that phosphomimetic mutations are a valuable substitute at least for simulations of phosphorylated cTn. Although it is interesting in its own right, this study is the third in a series of computational/experimental studies that have been able to show that the C-I interaction plays a crucial role in modulating the effects of phosphorylation and mutation.

We previously showed that with WT cTn, cTnI-S23D/S24D phosphomimetic mutations result in a reduction of C-I interactions and accelerate the early phase of relaxation in cardiac myofibrils (17). MD simulations showed that the cTnI-S23D/S24D mutations resulted in the formation of new intrasubunit contacts between the N-terminal extension and the inhibitory peptide of cTnI. We concluded from this that this new interaction could destabilize the cTnI switch peptide interaction with cTnC, resulting in the decreased C-I interaction and faster relaxation. Here, we demonstrate that this interaction does not occur when cTn contains cTnI-R145G. Thus, it may be that changes in the C-I interaction and early-phase relaxation with phosphorylation are blunted in the presence of the mutation, which may impair the early phase of diastole in hearts with this HCM-associated mutation.

SUPPORTING MATERIAL

Seven figures are available at [http://www.biophysj.org/biophysj/supplemental/S0006-3495\(14\)04674-8](http://www.biophysj.org/biophysj/supplemental/S0006-3495(14)04674-8).

ACKNOWLEDGMENTS

We thank the members of the McCammon group for useful discussions, and Drs. John Solaro and Paul Rosevear for structural information about the cTnI N-terminal extension.

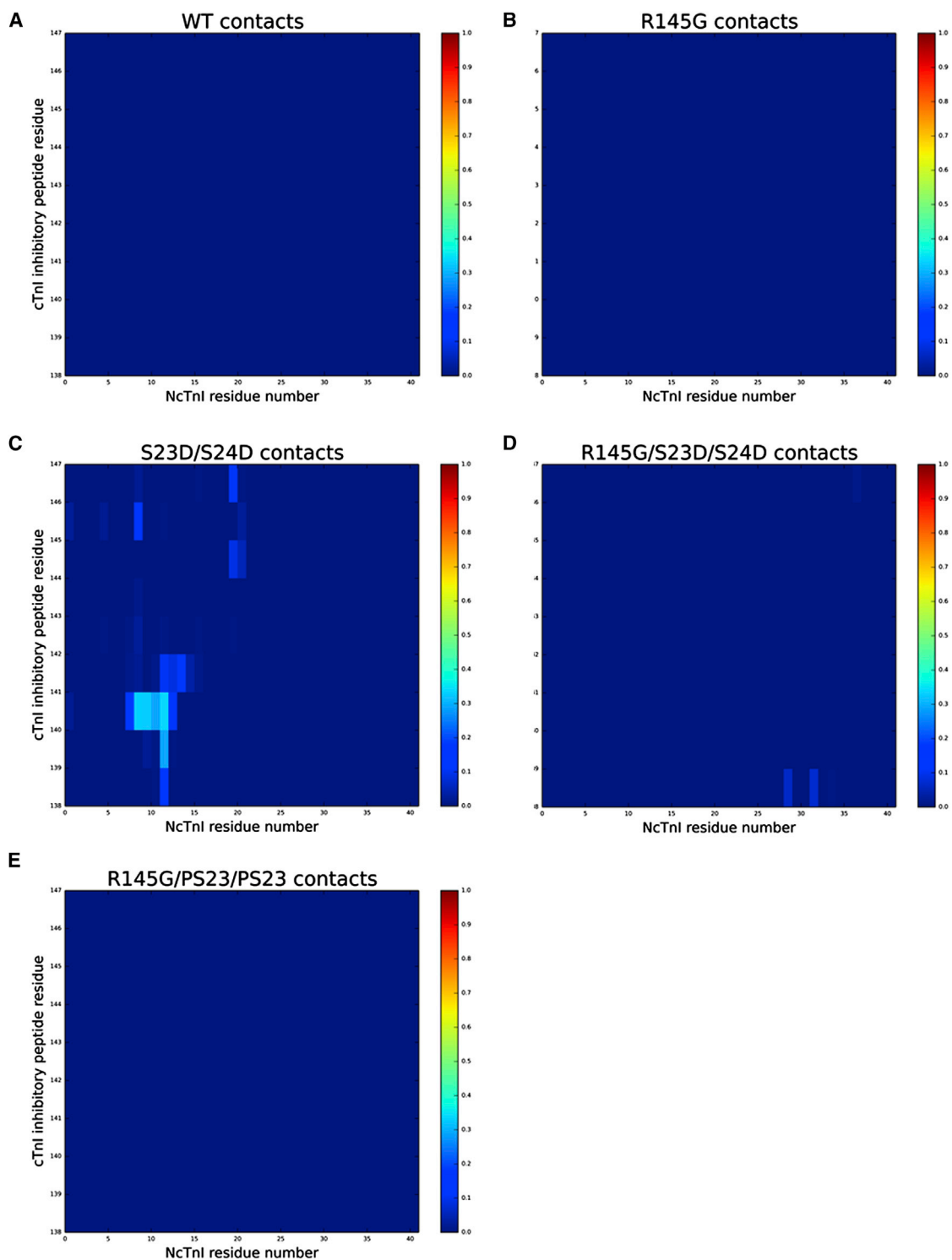


FIGURE 8 (A–E) Average contact map of residue-residue pairs between cTnI inhibitory peptide (cTnI residues 138–147) and NcTnI (cTnI residues 1–41) for (A) WT, (B) cTnI-R145G, (C) cTnI-S23D/S24D, (D) cTnI-R145G/S23D/S24D, and (E) cTnI-R145G/PS23/PS24 cTnI complexes.

This work was supported by the National Institutes of Health (HL111197 to M.R. and GM31749 to J.A.M.), the National Science Foundation (NSF), the Howard Hughes Medical Institute, the National Biomedical Computation Resource, and the NSF Supercomputer Centers. Computational resources

were supported in part by NSF grant PHY-0822283 to the Center for Theoretical Biological Physics. S.L. was supported by the American Heart Association (12POST11570005) and the Center for Theoretical Biological Physics. M.R. is an Established Investigator of the American Heart

Association. P.K.-H. received postdoctoral funding from the American Heart Association (13POST14510036) and the National Institutes of Health (1F32HL114365-01A1).

REFERENCES

- Li, M. X., X. Wang, and B. D. Sykes. 2004. Structural based insights into the role of troponin in cardiac muscle pathophysiology. *J. Muscle Res. Cell Motil.* 25:559–579.
- Farah, C. S., and F. C. Reinach. 1995. The troponin complex and regulation of muscle contraction. *FASEB J.* 9:755–767.
- Lindert, S., P. M. Kekenes-Huskey, and J. A. McCammon. 2012. Long-timescale molecular dynamics simulations elucidate the dynamics and kinetics of exposure of the hydrophobic patch in troponin C. *Biophys. J.* 103:1784–1789.
- Kobayashi, T., and R. J. Solaro. 2005. Calcium, thin filaments, and the integrative biology of cardiac contractility. *Annu. Rev. Physiol.* 67:39–67.
- Gordon, A. M., E. Homsher, and M. Regnier. 2000. Regulation of contraction in striated muscle. *Physiol. Rev.* 80:853–924.
- Colson, B. A., T. Bekyarova, ..., R. L. Moss. 2008. Protein kinase A-mediated phosphorylation of cMyBP-C increases proximity of myosin heads to actin in resting myocardium. *Circ. Res.* 103:244–251.
- Kentish, J. C., D. T. McCloskey, ..., R. J. Solaro. 2001. Phosphorylation of troponin I by protein kinase A accelerates relaxation and crossbridge cycle kinetics in mouse ventricular muscle. *Circ. Res.* 88:1059–1065.
- Zhang, R., J. Zhao, ..., J. D. Potter. 1995. Cardiac troponin I phosphorylation increases the rate of cardiac muscle relaxation. *Circ. Res.* 76:1028–1035.
- Rao, V., Y. Cheng, ..., M. Regnier. 2014. PKA phosphorylation of cardiac troponin I modulates activation and relaxation kinetics of ventricular myofibrils. *Biophys. J.* 107:1196–1204.
- Solaro, R. J., P. Rosevear, and T. Kobayashi. 2008. The unique functions of cardiac troponin I in the control of cardiac muscle contraction and relaxation. *Biochem. Biophys. Res. Commun.* 369:82–87.
- Kimura, A., H. Harada, ..., T. Sasazuki. 1997. Mutations in the cardiac troponin I gene associated with hypertrophic cardiomyopathy. *Nat. Genet.* 16:379–382.
- Deng, Y., A. Schmidtman, ..., R. Thieleczek. 2001. Effects of phosphorylation and mutation R145G on human cardiac troponin I function. *Biochemistry.* 40:14593–14602.
- Elliott, K., H. Watkins, and C. S. Redwood. 2000. Altered regulatory properties of human cardiac troponin I mutants that cause hypertrophic cardiomyopathy. *J. Biol. Chem.* 275:22069–22074.
- Takahashi-Yanaga, F., S. Morimoto, ..., I. Ohtsuki. 2001. Functional consequences of the mutations in human cardiac troponin I gene found in familial hypertrophic cardiomyopathy. *J. Mol. Cell. Cardiol.* 33:2095–2107.
- Kobayashi, T., W. J. Dong, ..., R. J. Solaro. 2004. Effects of protein kinase C dependent phosphorylation and a familial hypertrophic cardiomyopathy-related mutation of cardiac troponin I on structural transition of troponin C and myofilament activation. *Biochemistry.* 43:5996–6004.
- Kobayashi, T., and R. J. Solaro. 2006. Increased Ca²⁺ affinity of cardiac thin filaments reconstituted with cardiomyopathy-related mutant cardiac troponin I. *J. Biol. Chem.* 281:13471–13477.
- Cheng, Y., S. Lindert, ..., M. Regnier. 2014. Computational studies of the effect of the S23D/S24D troponin I mutation on cardiac troponin structural dynamics. *Biophys. J.* 107:1675–1685.
- Regnier, M., Y. Cheng, ..., A. McCulloch. 2014. *Biophys. J.* 106:221a. <http://dx.doi.org/10.1016/j.bpj.2013.11.1292>.
- Biesiadecki, B. J., T. Kobayashi, ..., P. P. de Tombe. 2007. The troponin C G159D mutation blunts myofilament desensitization induced by troponin I Ser23/24 phosphorylation. *Circ. Res.* 100:1486–1493.
- Dohet, C., E. al-Hillawi, ..., J. C. Ruegg. 1995. Reconstitution of skinned cardiac fibres with human recombinant cardiac troponin-I mutants and troponin-C. *FEBS Lett.* 377:131–134.
- Finley, N., M. B. Abbott, ..., P. R. Rosevear. 1999. NMR analysis of cardiac troponin C-troponin I complexes: effects of phosphorylation. *FEBS Lett.* 453:107–112.
- Hanft, L. M., B. J. Biesiadecki, and K. S. McDonald. 2013. Length dependence of striated muscle force generation is controlled by phosphorylation of cTnI at serines 23/24. *J. Physiol.* 591:4535–4547.
- Sakthivel, S., N. L. Finley, ..., J. Robbins. 2005. In vivo and in vitro analysis of cardiac troponin I phosphorylation. *J. Biol. Chem.* 280:703–714.
- Takimoto, E., D. G. Soergel, ..., A. M. Murphy. 2004. Frequency- and afterload-dependent cardiac modulation in vivo by troponin I with constitutively active protein kinase A phosphorylation sites. *Circ. Res.* 94:496–504.
- Wijnker, P. J., D. B. Foster, ..., J. van der Velden. 2013. Impact of site-specific phosphorylation of protein kinase A sites Ser23 and Ser24 of cardiac troponin I in human cardiomyocytes. *Am. J. Physiol. Heart Circ. Physiol.* 304:H260–H268.
- Yamasaki, R., Y. Wu, ..., H. Granzier. 2002. Protein kinase A phosphorylates titin's cardiac-specific N2B domain and reduces passive tension in rat cardiac myocytes. *Circ. Res.* 90:1181–1188.
- Takeda, S., A. Yamashita, ..., Y. Maéda. 2003. Structure of the core domain of human cardiac troponin in the Ca(2+)-saturated form. *Nature.* 424:35–41.
- Jacobson, M. P., R. A. Friesner, ..., B. Honig. 2002. On the role of the crystal environment in determining protein side-chain conformations. *J. Mol. Biol.* 320:597–608.
- Jacobson, M. P., D. L. Pincus, ..., R. A. Friesner. 2004. A hierarchical approach to all-atom protein loop prediction. *Proteins.* 55:351–367.
- Rohl, C. A., C. E. Strauss, ..., D. Baker. 2004. Modeling structurally variable regions in homologous proteins with rosetta. *Proteins.* 55:656–677.
- Sood, V. D., and D. Baker. 2006. Recapitulation and design of protein binding peptide structures and sequences. *J. Mol. Biol.* 357:917–927.
- Manning, E. P., J. C. Tardiff, and S. D. Schwartz. 2011. A model of calcium activation of the cardiac thin filament. *Biochemistry.* 50:7405–7413.
- Humphrey, W., A. Dalke, and K. Schulten. 1996. VMD: visual molecular dynamics. *J. Mol. Graphics.* 14:33–38, 27–38.
- MacKerell, Jr., A. D., N. Banavali, and N. Foloppe. 2000–2001. Development and current status of the CHARMM force field for nucleic acids. *Biopolymers.* 56:257–265.
- Phillips, J. C., R. Braun, ..., K. Schulten. 2005. Scalable molecular dynamics with NAMD. *J. Comput. Chem.* 26:1781–1802.
- Ryckaert, J.-P., G. Ciccotti, and H. J. C. Berendsen. 1977. Numerical integration of the cartesian equations of motion of a system with constraints: molecular dynamics of n-alkanes. *J. Comput. Phys.* 23:327–341.
- Wang, D., I. M. Robertson, ..., M. Regnier. 2012. Structural and functional consequences of the cardiac troponin C L48Q Ca(2+)-sensitizing mutation. *Biochemistry.* 51:4473–4487.
- Zou, X. Q., Y. X. Sun, and I. D. Kuntz. 1999. Inclusion of solvation in ligand binding free energy calculations using the generalized-Born model. *J. Am. Chem. Soc.* 121:8033–8043.
- Hou, T., J. Wang, ..., W. Wang. 2011. Assessing the performance of the molecular mechanics/Poisson Boltzmann surface area and molecular mechanics/generalized Born surface area methods. II. The accuracy of ranking poses generated from docking. *J. Comput. Chem.* 32:866–877.
- Still, W. C., A. Tempczyk, ..., T. Hendrickson. 1990. Semianalytical treatment of solvation for molecular mechanics and dynamics. *J. Am. Chem. Soc.* 112:6127–6129.

41. Tanner, D. E., K. Y. Chan, ..., K. Schulten. 2011. Parallel generalized Born implicit solvent calculations with NAMD. *J. Chem. Theory Comput.* 7:3635–3642.
42. Onufriev, A., D. Bashford, and D. A. Case. 2004. Exploring protein native states and large-scale conformational changes with a modified generalized Born model. *Proteins.* 55:383–394.
43. Tsui, V., and D. A. Case. 2000-2001. Theory and applications of the generalized Born solvation model in macromolecular simulations. *Biopolymers.* 56:275–291.
44. Weiser, J., P. S. Shenkin, and W. C. Still. 1999. Approximate atomic surfaces from linear combinations of pairwise overlaps (LCPO). *J. Comput. Chem.* 20:217–230.
45. Qiu, D., P. S. Shenkin, ..., W. C. Still. 1997. The GB/SA continuum model for solvation. A fast analytical method for the calculation of approximate Born radii. *J. Phys. Chem. A.* 101:3005–3014.
46. Gohlke, H., and D. A. Case. 2004. Converging free energy estimates: MM-PB(GB)SA studies on the protein-protein complex Ras-Raf. *J. Comput. Chem.* 25:238–250.
47. Hwang, P. M., F. Cai, ..., B. D. Sykes. 2014. The cardiac-specific N-terminal region of troponin I positions the regulatory domain of troponin C. *Proc. Natl. Acad. Sci. USA.* 111:14412–14417.
48. Manning, E. P., J. C. Tardiff, and S. D. Schwartz. 2012. Molecular effects of familial hypertrophic cardiomyopathy-related mutations in the TNT1 domain of cTnT. *J. Mol. Biol.* 421:54–66.
49. Zhou, Z., D. Rieck, ..., W. J. Dong. 2013. Structural and kinetic effects of hypertrophic cardiomyopathy related mutations R146G/Q and R163W on the regulatory switching activity of rat cardiac troponin I. *Arch. Biochem. Biophys.* 535:56–67.
50. Beard, H., A. Cholleti, ..., K. A. Loving. 2013. Applying physics-based scoring to calculate free energies of binding for single amino acid mutations in protein-protein complexes. *PLoS ONE.* 8:e82849.
51. Varughese, J. F., T. Baxley, ..., Y. Li. 2011. A computational and experimental approach to investigate bepridil binding with cardiac troponin. *J. Phys. Chem. B.* 115:2392–2400.
52. Wang, B., L. Li, ..., S. O. Meroueh. 2013. Molecular recognition in a diverse set of protein-ligand interactions studied with molecular dynamics simulations and end-point free energy calculations. *J. Chem. Inf. Model.* 53:2659–2670.
53. Fenley, A. T., H. S. Muddana, and M. K. Gilson. 2012. Entropy-enthalpy transduction caused by conformational shifts can obscure the forces driving protein-ligand binding. *Proc. Natl. Acad. Sci. USA.* 109:20006–20011.
54. Kruger, M., S. Zittrich, ..., R. Stehle. 2005. Effects of the mutation R145G in human cardiac troponin I on the kinetics of the contraction-relaxation cycle in isolated cardiac myofibrils. *J. Physiol.* 564:347–357.
55. Kekenus-Huskey, P. M., S. Lindert, and J. A. McCammon. 2012. Molecular basis of calcium-sensitizing and desensitizing mutations of the human cardiac troponin C regulatory domain: a multi-scale simulation study. *PLOS Comput. Biol.* 8:e1002777.
56. Howarth, J. W., J. Meller, ..., P. R. Rosevear. 2007. Phosphorylation-dependent conformational transition of the cardiac specific N-extension of troponin I in cardiac troponin. *J. Mol. Biol.* 373:706–722.
57. Sadayappan, S., N. Finley, ..., J. Robbins. 2008. Role of the acidic N' region of cardiac troponin I in regulating myocardial function. *FASEB J.* 22:1246–1257.